Journal of Alloys and Compounds, 197 (1993) 57–64
JALCOM 629

Condensed tetrakaidecahedral clusters. The crystal structure of $NiTa_8Se_8$*

Matthias Conrad and Bernd Harbrecht**
Institut für Anorganische Chemie, Universität Bonn, Bonn (Germany)

(Received December 12, 1992)

Abstract

The ternary selenides MTa_8Se_8 (M ≡ Co, Ni) were prepared from compacted, pre-reacted mixtures of the elemental components. Coarse crystalline $NiTa_8Se_8$ was obtained from reactions performed in sealed molybdenum crucibles at 1620 K for 2 days with the use of iodine as a transport agent. The selenides crystallize in space group type *Pnma* with four formula units per unit cell. The lattice parameters are $a = 2241.3(1)$ pm, $b = 344.22(3)$ pm, $c = 1684.1(1)$ pm and $a = 2247.4(2)$ pm, $b = 342.72(3)$ pm, $c = 1690.3(1)$ pm for $NiTa_8Se_8$ and $CoTa_8Se_8$ respectively. The structure of $NiTa_8Se_8$ was determined from X-ray intensities of a single crystal and refined to $R(I) = 0.040$ for 1411 structure factors and 104 variables. The highly porous intermetallic partial structure contains columns of face-shared, Ni-centred $NiTa_9$ tetrakaidecahedra which are covered by selenium atoms exhibiting a one-sided coordination with three, four or five tantalum atoms as nearest neighbours. $NiTa_8Se_8$ is a metallic conductor.

1. Introduction

In recent years preparative investigations aimed at the synthesis of tantalum-rich chalcogenides have produced a variety of new binary and ternary materials with unexpected structural properties. One of the surprises concerns the importance of van der Waals interactions for the architecture of several of the solids. Thus Ta_2Te_3 [1], $MTaTe_2$ (M ≡ Fe, Co, Ni) [2], Ta_2Se [3] and $(Nb,Ta)_5S_2$ [4], for example, form distinct layered structures. However, there are also materials for which strong bonding interactions are restricted to extended columnar clusters. The tellurides Ta_4SiTe_4 [5] and Ta_6Te_5 [6] are prominent representatives of novel quasi-one-dimensional compounds comprised of centred tetragonal and pentagonal Ta antiprisms which are fused into columns according to $^1_\infty[SiTa_{8/2}Te_4]$ and $^1_\infty[TaTa_{10/2}Te_5]$ respectively.

The discoveries also include sulphides $M_2Ta_9S_6$ [7] and selenides $M_2Ta_{11}Se_8$ [8] containing an iron group metal M ≡ Fe, Co, Ni as a minor third component. The shaping structural motifs of these compounds are M-centred tricapped trigonal prisms, *i.e.* strongly metal-bonded MTa_9 tetrakaidecahedra which are condensed at opposed triangular prism faces to form columns $^1_\infty[MTa_{6/2}Ta_3]$. Further fusion of these columnar units at all three capping positions leads to a highly porous three-dimensional intermetallic core $^3_\infty[MTa_{6/2}Ta_{3/2}]$ as present in $M_2Ta_9S_6$ [7]. Compared with the tantalum sulphides, the degree of condensation of the columnar units is increased for $M_{2-x}Nb_8S_{4+x}$ (M ≡ Co, Ni) [9]. As seen from Fig. 1, the intermetallic framework of the niobium sulphides consists of tetrakaidecahedral columns sharing both edges and vertices. Conversely, the selenides $M_2Ta_{11}Se_8$ are less metal rich than the tantalum sulphides, the degree of condensation being reduced. The intermetallic columnar cores have only one out of three capping positions in common. The "twin columns" $^1_\infty[MTa_{6/2}Ta_{1/2}Ta_2]$ are coupled to four equivalent units mainly by bridging Se atoms.

In view of the conspicuous relations existing between the structure and composition of these ternary chalcogenides, the question arises as to whether low-dimensional materials based on condensed tetrakaidecahedral clusters can be prepared too. For example, the composition of a compound composed of uncoupled intermetallic columns of condensed MTa_9 tetrakaidecahedra $^1_\infty[MTa_{6/2}Ta_3]$ would be MTa_6Q_6 if the columnar units were as completely covered at the periphery by Q as the Ta cores of Ta_4SiTe_4 and Ta_6Te_5 are covered by Te (see Fig. 2).

In the course of our attempts to synthesize such ternaries which are less metal-rich than $M_2Ta_{11}Se_8$, we found new ternary selenides of composition MTa_8Se_8 (M ≡ Co, Ni) which are the subject of this report.

*Dedicated to Professor Dietrich Mootz on the occasion of his 60th birthday.

**Author to whom correspondence should be addressed.

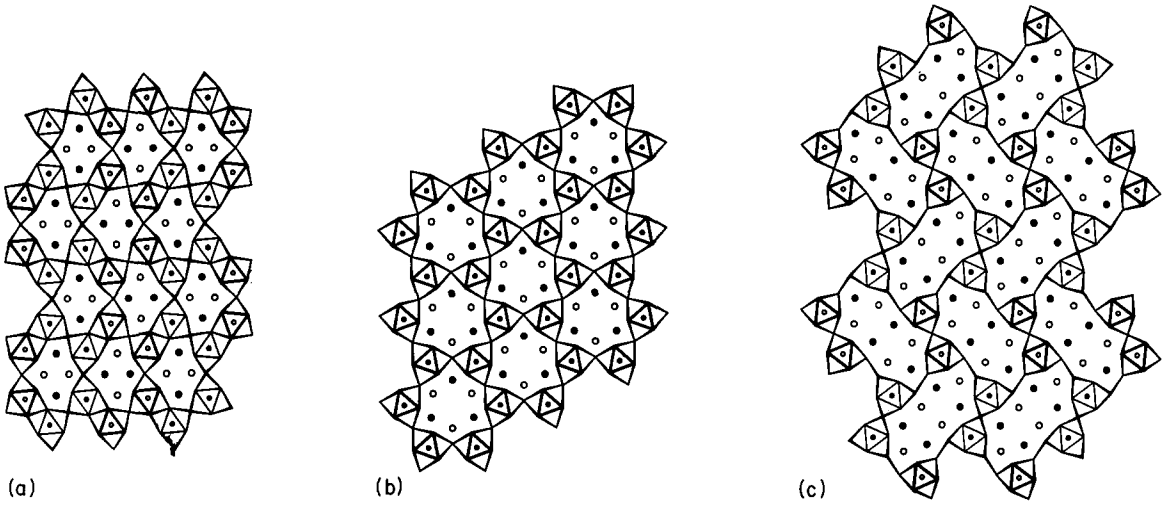

Fig. 1. Structures of (a) $M_{2-x}Nb_8S_{4+x}$, (b) $M_2Ta_9S_6$ and (c) $M_2Ta_{11}Se_8$ projected along the short crystallographic axis with emphasis on the group V metal network.

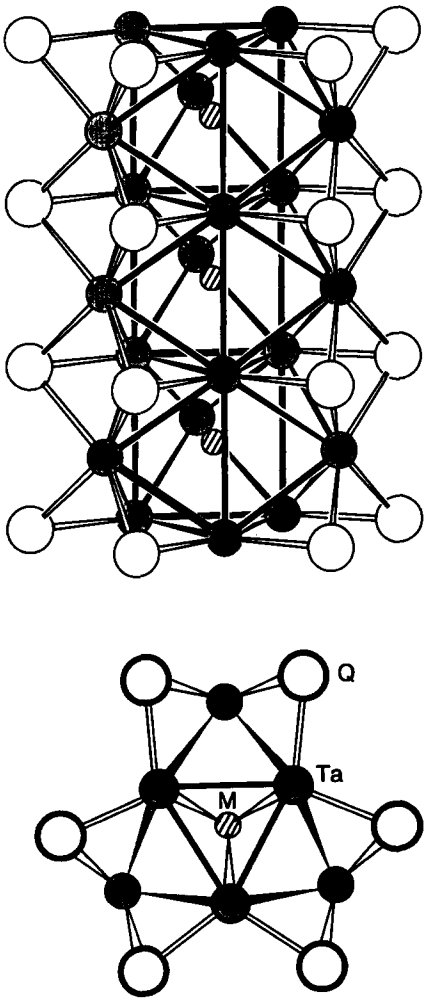

Fig. 2. View of a $^1_\infty[MTa_{6/2}Ta_{3Q6}]$ column as expected for composition MTa_6Q_6.

2. Synthesis

The origin and purity of the elements used for the reactions have been described before [8]. The first indication of a second tantalum-rich cobalt selenide was obtained from reactions of 1 g mixtures of the elements in the ratio n(Co):n(Ta):n(Se) = 1:6:5. The reactions were performed in the presence of iodine (about 2 mg cm^{-3}) in previously outgassed, double-walled quartz glass ampoules at 1450 K for 1 day. The nickel compound which turned out to be $NiTa_8Se_8$ was obtained under similar conditions. Attempts to synthesize the iron compound have failed so far. The samples prepared by this route consisted of bunches of fibres which were several millimetres long but hardly more than 1 μm thick (Fig. 3).

Rather pure samples of $NiTa_8Se_8$ were obtained from stoichiometric mixtures of the elements which were pre-reacted in evacuated and sealed silica tubes at 1200 K for 0.5 h. Subsequently, the grounded and pelletized products were heated in a vacuum ($p < 10^{-3}$ Pa) at 1600 K for 12 h using molybdenum or alumina crucibles as containers. The intermediate steps had to be carried out in a glove-box under an argon atmosphere; otherwise traces of Ta_2O_5 were formed in the subsequent reaction. This route yielded microcrystalline, black powders.

Crystals of suitable size for conventional X-ray diffraction experiments were grown by heating the pre-reacted mixture in the presence of iodine in a sealed molybdenum crucible for 2 days at 1620 K. The product consisted of needle- or slat-shaped crystals of metallic lustre. The crystals could easily be cleaved parallel to the needle axis.

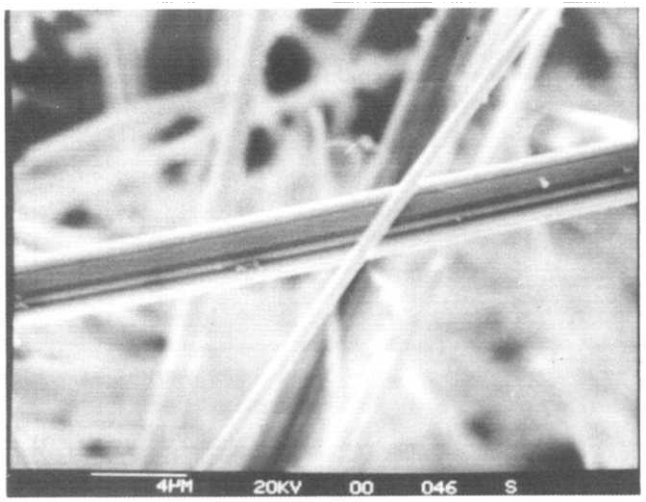

(a)

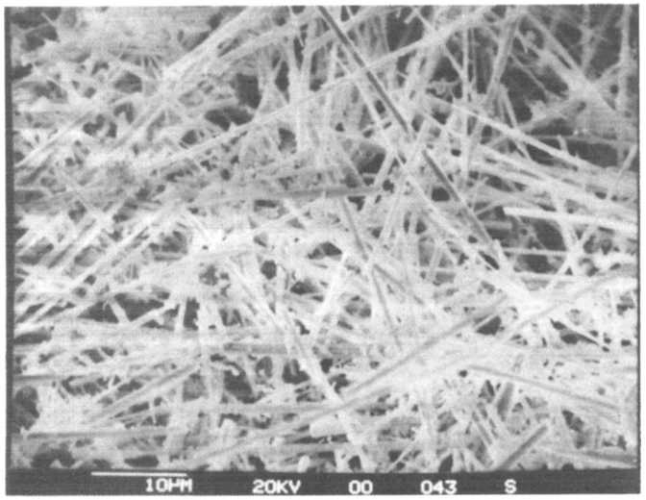

(b)

Fig. 3. SEM images of $NiTa_8Se_8$ crystals.

Semiquantitative analyses of the crystals by energy-dispersive analysis of X-rays (EDX; PV 9800, Edax) in a scanning electron microscope (SEM; DSM 940, Zeiss) confirmed the composition (exp. (calc.): 6.0 (5.88) at.% Ni, 47.0 (47.06) at.% Ta, 47.0 (47.06) at.% Se) and did not show any contamination by molybdenum or iodine.

Investigations of the stability range of MTa_8Se_8 revealed that the compounds disproportionate at high temperature. $NiTa_8Se_8$ decomposes at temperatures between 1800 and 1900 K. $Ni_2Ta_{11}Se_8$ and $Ta_{1+x}Se_2$ are the major components. The selenides are not stable in air; they decompose within a few days if not stored under an inert atmosphere.

3. X-Ray diffraction

The phases were identified by means of X-ray powder diffraction. Samples containing admixed silicon [10] as an internal standard were exposed to Cu $K\alpha_1$ radiation in a Guinier camera (FR 552, Enraf Nonius, Delft, Netherlands). The Guinier patterns of the new phases were indexed taking into consideration the calculated diffraction angles and intensities (program LAZY PULVERIX [11]) derived from parameters of the single-crystal X-ray structure determination of $NiTa_8Se_8$. Diffraction angles and estimated and calculated relative intensities are listed in Table 1; lattice parameters are given in Table 2.

TABLE 1. Low angle Guinier data (Cu $K\alpha_1$) of $NiTa_8Se_8$

$h\ k\ l$	$\sin^2\theta\times10^5$		I_{rel}	
	Calc.	Obs.	Calc.	Estim.
2 0 0	472	465	29	w
2 0 1	682	675	100	m
0 0 2	837	832	4	vw
1 0 2	955	940	1	vw
3 0 1	1272	1263	35	m
2 0 2	1309	1300	42	m
4 0 0	1890	1881	5	vw
1 0 3	2001	1989	7	w
4 0 1	2099	2088	21	w
2 0 3	2355	2342	5	vw
4 0 2	2726	2720	8	w
3 0 3	2946	2933	4	vw
5 0 1	3162	3155	4	vw
1 0 4	3465	3460	1	vw
2 0 4	3819	3807	2	vw
3 0 4	4410	4405	1	vw
6 0 1	4461	4450	1	vw
5 0 3	4835	4827	1	vw
0 1 1	5217	5204	3	w
1 1 1	5335	5331	1	vw
2 1 0	5480	5469	1	vw
2 1 1	5689	5685	1	vw
1 1 2	5962	5951	1	vw
6 0 3	6135	6123	2	vw
3 1 1	6279	6275	13	m
7 0 2	6624	6613	2	vw
3 1 2	6907	6903	3	w
1 1 3	7008	6998	5	w
4 1 1	7106	7099	3	w
2 1 3	7362	7359	3	w
8 0 0	7559	7555	2	vw
7 0 3	7670	7664	10	vw
4 1 2	7734	7722	40	s
3 1 3	7953	7946	8	vw
2 0 6	8003	7999	17	w
5 1 1	8169	8166	2	vw
1 1 4	8472	8467	52	s
3 0 6	8594	8590	1	vw
4 1 3	8780	8780	5	vw
5 1 2	8797		3	
2 1 4	8827	8817	17	w
7 0 4	9134	9129	10	w
3 1 4	9417	9415	4	w
6 0 5	9482	9472	14	w
5 1 3	9843	9833	48	s
6 1 2	10096	10101	6	w
0 1 5	10237	10234	8	w
4 1 4	10244		1	

TABLE 2. Lattice parameters (Guinier data, Cu $K\alpha_1$ radiation, silicon internal standard)

$CoTa_8Se_8$	$a = 2247.4(2)$ pm
	$b = 342.72(3)$ pm
	$c = 1690.3(1)$ pm
$NiTa_8Se_8$	$a = 2241.3(1)$ pm
	$b = 344.22(3)$ pm
	$c = 1684.1(1)$ pm

TABLE 3. Data collection and structure calculation of $NiTa_8Se_8$

Chemical formula	$NiTa_8Se_8$
Space group type	*Pnma* (No. 62)
a	22.402(4) pm
b	3.4422(3) pm
c	16.828(3) pm
V	1297.6(3) pm
Z	4
ρ_{calc}	10.944 g cm^{-1}
Molar mass	2137.97 g mol^{-1}
μ(Mo Kα)	900.1 cm^{-1}
Crystal size	$3\times150\times9$ μm^3
X-rays, monochromator	Mo Kα, graphite
Scan type	ω–2θ
Min., max. transmission	0.65, 1.00
Octants measured	$\pm h\ k\ \pm l$, $h\ -k\ l$
(θ range)	(0°–20°)
	$\pm h\ k\ l$ (20°–35°)
Number of reflections	
Measured	9244
Symmetry independent	3413
Symmetry independent with $I_o > 2.5\sigma(I_o)$	1411
Number of variables	104
$R_{int}(I_o > 3\sigma(I_o))$	0.047
$R(I)$, $R_w(I)$	0.040, 0.045
$R(F)$, $R_w(F)$	0.027, 0.023
$R(I)$ for all reflections	0.092
Goodness of fit, GOF	0.704
Secondary extinction coefficient	1.13×10^{-8}
$\Delta\rho_{max}$, $\Delta\rho_{min}$	5.52, -3.87×10^{-6} e pm^{-3}

TABLE 4. Positional parameters and equivalent displacement parameters B_{eq} (10^4 pm^2) of $NiTa_8Se_8$

Atom	Position	x	y	z	B_{eq}
Ta1	4c .m.	0.01909(3)	¼	0.16384(5)	0.42(1)
Ta2	4c .m.	0.44218(4)	¼	0.18059(4)	0.42(1)
Ta3	4c .m.	0.37528(4)	¼	0.34259(5)	0.41(1)
Ta4	4c .m.	0.04506(3)	¼	0.95852(4)	0.37(1)
Ta5	4c .m.	0.44482(4)	¼	0.80424(4)	0.45(1)
Ta6	4c .m.	0.16740(3)	¼	0.70844(5)	0.40(1)
Ta7	4c .m.	0.31545(4)	¼	0.06085(5)	0.53(1)
Ta8	4c .m.	0.24570(3)	¼	0.44693(5)	0.40(1)
Ni	4c .m.	0.0539(1)	¼	0.7901(2)	0.65(4)
Se1	4c .m.	0.42587(9)	¼	0.5688(1)	0.44(3)
Se2	4c .m.	0.12204(9)	¼	0.2317(1)	0.57(3)
Se3	4c .m.	0.03129(9)	¼	0.4138(1)	0.50(3)
Se4	4c .m.	0.09808(9)	¼	0.5753(1)	0.48(3)
Se5	4c .m.	0.26381(9)	¼	0.6042(1)	0.53(3)
Se6	4c .m.	0.26766(9)	¼	0.2867(1)	0.47(3)
Se7	4c .m.	0.33549(9)	¼	0.9089(1)	0.50(3)
Se8	4c .m.	0.16283(8)	¼	0.9504(1)	0.41(3)

TABLE 5. Anisotropic displacement parameters B_{ij} (10^4 pm^2) of $NiTa_8Se_8$ ($B_{12} = B_{23} = 0$)

Atom	B_{11}	B_{22}	B_{33}	B_{13}
Ta1	0.41(2)	0.40(3)	0.44(2)	0.03(2)
Ta2	0.42(2)	0.42(2)	0.42(2)	0.01(2)
Ta3	0.45(2)	0.43(3)	0.36(2)	0.03(2)
Ta4	0.27(2)	0.39(3)	0.45(2)	0.02(2)
Ta5	0.41(2)	0.44(2)	0.48(2)	0.02(2)
Ta6	0.42(2)	0.38(3)	0.41(2)	0.04(2)
Ta7	0.54(2)	0.53(3)	0.51(2)	−0.02(2)
Ta8	0.36(2)	0.45(3)	0.40(2)	0.02(2)
Ni	0.57(7)	0.75(9)	0.64(8)	0.20(8)
Se1	0.52(5)	0.31(7)	0.50(6)	−0.07(5)
Se2	0.44(6)	0.41(7)	0.87(7)	0.11(6)
Se3	0.55(6)	0.50(7)	0.45(5)	0.08(6)
Se4	0.43(6)	0.49(7)	0.52(6)	−0.07(5)
Se5	0.54(6)	0.45(7)	0.62(6)	−0.01(5)
Se6	0.42(6)	0.42(7)	0.56(6)	0.00(5)
Se7	0.47(6)	0.52(7)	0.52(6)	−0.03(6)
Se8	0.34(5)	0.28(6)	0.63(6)	0.10(5)

For the structure determination a crystal of dimensions $3\times150\times9$ μm^3 bounded by faces $\pm(2\,0\,1)$, $\pm(0\,1\,0)$ and $\pm(1\,0\,-1)$ was selected and fixed in a glass capillary 0.1 mm wide which was subsequently sealed under argon. The rotational symmetry and extinctions of zero- and first-level Weissenberg (Cu Kα) and precession (Mo Kα) exposures were consistent with space group types *Pnma* and $Pna2_1$ respectively. Data were collected on a Nonius CAD4 diffractometer using monochromatized Mo Kα radiation. No decay of intensities with time was observed. Absorption effects were corrected on the basis of Ψ scan data of six reflections. Merging of data led to $R_{int}(I_o) = 0.047$. The structure was solved using direct methods. A scale factor, positional and anisotropic thermal parameters as well as a coefficient for an extinction correction were refined in a full-block least-squares refinement by minimizing $\Sigma[1/\sigma^2(I_o)][(I_o - I_c)^2$ for all reflections with $I_o > 2.5\sigma(I_o)$. The refinement converged at $R(I) = 0.040$. The highest relative residual electron density $\Delta\rho_{max}/\rho_{max}(Ni) = 0.04$ was 75 pm distant from Ta5. The structure calculations were carried out using the structure determination package SDP (Enraf Nonius) running on a Vaxstation 4000. Crystal data, data collection parameters and structure refinement data are summarized in Table 3. Atom positions and displacement parameters are given in Tables 4 and 5.

4. Electrical resistivities

Electrical resistivities of microcrystalline $NiTa_8Se_8$ were measured in the temperature range 17–310 K using a heatable cold head D105 (Cryo Physics) connected to a closed-cycle helium cryostat and a temperature controller 330 (Lake Shore). Four copper wires were attached to a compacted disc consisting of $NiTa_8Se_8$. The contacts were made with silver paste and arranged linearly [12]. The outer wires were connected to a d.c. current generator TR6142 (Advantest). The decay of the voltage was measured between the two inner contacts. The large internal resistivity of the digital multimeter 195A (Keithley) guaranteed the elimination of the contact resistivities. Contributions of the thermoelectric power to the voltage were eliminated by changing the direction of the current for each temperature at which the resistivity was measured. The temperature was changed stepwise (2–5 K) and held constant within ± 0.2 K for at least 60 s before the voltage was registered to an accuracy of ± 0.2 μV. The resistivity ρ was calculated from the relationship $\rho = RA/l$, where $R(\Omega)$ is the electrical resistance, A (cm^2) is the cross-sectional area and l (cm) is the separation of the inner contacts. The estimated uncertainty in the measurements of the length is about $\pm 5 \times 10^{-3}$ cm. According to measurements of ρ(Ta) by the same method, the uncertainty $\Delta\rho/\rho$ is assumed to be ± 0.5. As shown in Fig. 4, the resistivity of $NiTa_8Se_8$ decreases steadily with decreasing temperature. There is no indication of any electronic instability between 17 and 310 K.

5. Discussion

The structure of $NiTa_8Se_8$ is built up by 17 crystallographically distinct atoms (Ni, Ta1 to Ta8, Se1 to Se8), all of which are situated in mirror planes at heights $y = \frac{1}{4}, \frac{3}{4}$ of space group type *Pnma*. Figure 5 shows part of the structure projected along ***b***. An extended portion of the structure is depicted in Fig. 6; characteristic distances are listed in Table 6.

The intermetallic core of $NiTa_8Se_8$ is comprised of Ni–Ta (mean distance ⟨250.8 pm⟩ (6×), ⟨288.2 pm⟩ (3×)) and Ta–Ta (299.5–322.4 pm) bonded $NiTa_9$ tetrakaidecahedra fused into columns by common triangulated prism faces (Ta1–Ta3). The extended intermetallic units $^1_\infty[NiTa_{6/2}Ta_3]$ are pairwise linked to each other at one (Ta4; 298.8 pm) out of three (Ta4 to Ta6) capping sites of condensed prisms $^1_\infty[NiTa_{6/2}Ta_3]$. The intermetallic columns coupled by a twofold screw operation are shifted relative to each other by *b*/2, *i.e.* by half the height of a tetrakaidecahedron along its pseudothreefold axis of symmetry. There are two more tantalum sites, Ta7 and Ta8, completing the highly porous intermetallic partial structure. Ta7 is bonded to two Ta6 (304.6 pm) and to Ta8, which in turn has only two Ta7 as nearest metal neighbours (291.8 pm) whereas Ta3 of another column is already 332.2 pm distant.

Assuming that this distance is not indicative of any substantial Ta–Ta interaction, especially since Se6 and two Se8 bridge the Ta3–Ta8 pairs, then the Ni–Ta and Ta–Ta bonding regions are restricted to quasi-one-dimensional arrays of condensed and linked $NiTa_9$ tetrakaidecahedra to which Ta7 and Ta8 are additionally bonded. It may be remarked that these two "extra" tantalum sites together with Ta6 constitute a fragment of a second column of condensed tricapped trigonal prisms which lacks (i) two positions in the prism triangles, (ii) one capping position and (iii) the 3d metal chain in the centre of the column. A quite similar fragment is formed by *e.g.* Ta1, Ta4 and Ta5. Thus the extended intermetallic unit of $NiTa_8Se_8$ can be considered as a specific fragment of a "twin column" $^1_\infty[NiTa_{6/2}Ta_2Ta_{1/2}]$ as present in $Ni_2Ta_{11}Se_8$ (see Fig. 1(c)).

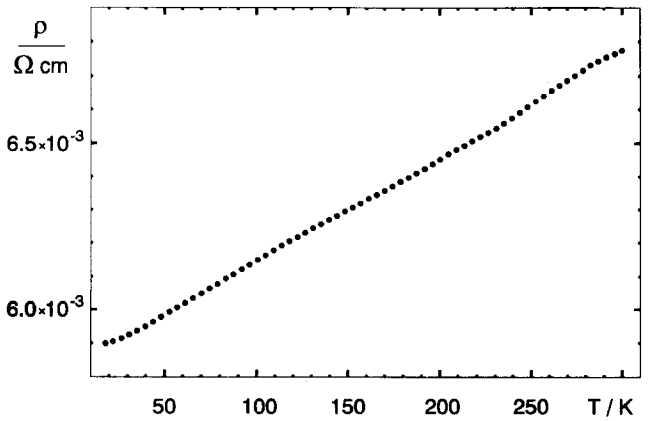

Fig. 4. Resistivity of $NiTa_8Se_8$ as a function of temperature.

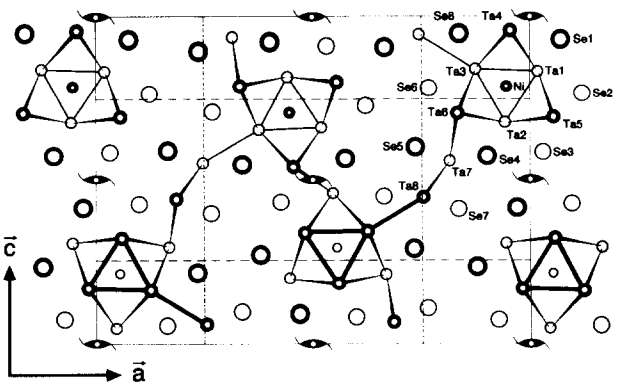

Fig. 5. Part of the structure of $NiTa_8Se_8$ projected on to (010) (thin line circles, $y = \frac{1}{4}$; bold line circles, $y = \frac{3}{4}$).

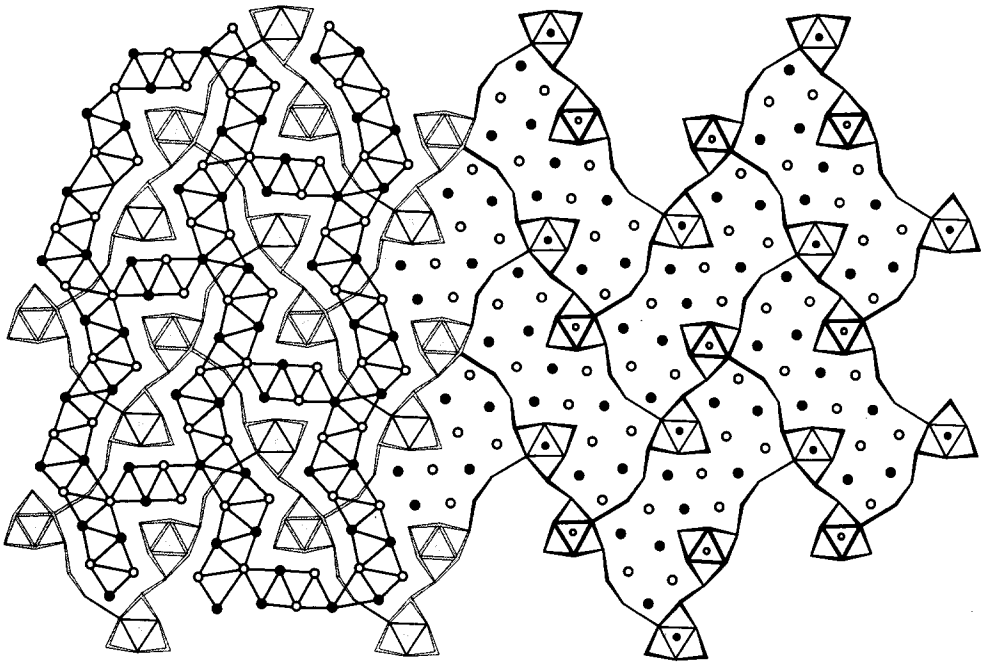

Fig. 6. Projection of the structure of $NiTa_8Se_8$ along [010] with emphasis on the Ta network (at the right) and the octahedral Se framework in which the intermetallic cores $NiTa_{6/2}Ta_3$ are embedded (left).

The selenium atoms cover the internal surface of the open intermetallic framework. They strongly interact exclusively with tantalum atoms ($d_{Se-Se} > 310$ pm, $d_{Ni-Se} > 363$ pm). Ta8 at the outer side of the fragment is enclosed in a distorted Se6 octahedron (⟨265.7 pm⟩) in addition to being in close contact with two Ta7 (291.8 pm). Similar coordinations and distances are found for Ta1 in Ta_2Se_3 [13] ($d_{Ta1-Ta1} = 292$ pm (2×), $d_{Ta-Se} = ⟨263.5$ pm⟩ (6×)). Ta7 may have a larger valence electron concentration available for homonuclear bonding than Ta8: Ta7 is in bonding contact with two Ta8 and two Ta6 (304.6 pm) and has only five selenium atoms as neighbours (⟨259.2 pm⟩). Ta6, Ta5 and Ta4 are each situated above the rectangular prism faces. They all have four selenium atoms as neighbours at a mean distance of ⟨263.7 pm⟩. In addition, Ta5 has four and Ta4 and Ta6 each have six tantalum atoms as neighbours at ⟨305.3 pm⟩ and ⟨304.5 pm⟩ respectively. Ta1, Ta2 and Ta3 constitute the columns of face-shared prisms and interact strongly with the nickel atoms in the centre of the prisms (⟨250.8 pm⟩). They are bonded to three selenium atoms (⟨261.8 pm⟩). Obviously, these tantalum atoms have the highest valence electron concentration left for the formation of hetero- and homonuclear metal–metal bonds.

The specific Ta–Se bonding interactions are also reflected in the coordinations about the various selenium atoms which have coordination numbers (CNs) ranging from three to five. Se2 and Se3 (CN = 3, ⟨257.6 pm⟩) link two face-shared $NiTa_9$ clusters at the peripheral position Ta5. Se6 (CN = 4, ⟨263.7 pm⟩) bridges two clusters in a similar way and, like Se8, is bonded to an outer Ta8 of a fragment of a second column. In addition, Se8 (CN = 5, ⟨265.6 pm⟩) covers a triangular face of a tetrakaidecahedron. Se1 and Se4, being square pyramidal coordinated (CN = 5, ⟨264.3 pm⟩), also cover peripheral faces of the tetrakaidecahedra. Se7 has only weak contact with the $NiTa_9$ cluster ($d_{Ta5-Se7} = 301.6$ pm). It is strongly bonded to three "extra" tantalum atoms (two Ta8, one Ta7, ⟨258.9 pm⟩). It may be remarked that irrespective of the specific coordinations all selenium atoms are coordinated only at one side, as expected for atoms covering a surface. Moreover, the various coordinations about selenium atoms resemble fragments of fictitious Ta_9Se tetrakaidecahedra. As illustrated in Fig. 7, there are two topologically different configurations about selenium atoms with four and five tantalum atoms as neighbours respectively.

Another structural feature of $NiTa_8Se_8$ concerns the existence of void regions which are associated with the one-sided coordination about the selenium atoms. Se1, Se2 and Se5 to Se8 are arranged in puckered double layers parallel to (100) composed of distorted nonbonded Se_6 octahedra sharing edges. This structural feature is emphasized in the left part of Fig. 6. Every third column of edge-shared Se_6 octahedra is centred by Ta8. The double layers are spatially linked by columns of condensed Se_6 octahedra which are formed by Se3, Se4 and Se7. The shortest Se–Se distances occur in this region between Se3 and Se4 at the same elevations (310.8 pm). Although this distance is about 10% shorter than the mean distance between other selenium atoms

TABLE 6. Characteristic interatomic[a] distances (pm) of $NiTa_8Se_8$

Ta1–	Ta5	(2×)	303.3(1)	Ta5–	Ta1	(2×)	303.3(1)
	Ta4	(2×)	304.4(1)		Ta2	(2×)	307.2(1)
	Ta2	(1×)	313.4(1)		Ni	(1×)	291.3(3)
	Ta3	(1×)	322.4(1)		Se3	(2×)	257.8(2)
	Ta4	(1×)	350.4(1)		Se2	(2×)	258.8(2)
	Ni	(2×)	249.7(2)		Se7	(1×)	301.6(2)
	Se2	(1×)	257.4(2)				
	Se1	(2×)	265.4(2)	Ta6–	Ta3	(2×)	299.5(1)
					Ta2	(2×)	303.4(1)
Ta2–	Ta6	(2×)	303.4(1)		Ta7	(2×)	304.6(1)
	Ta5	(2×)	307.2(1)		Ni	(1×)	289.1(3)
	Ta3	(1×)	311.1(1)		Se6	(2×)	261.1(2)
	Ta1	(1×)	313.4(1)		Se4	(1×)	272.5(2)
	Ta7	(1×)	348.1(1)		Se5	(1×)	278.2(2)
	Ni	(2×)	252.3(2)				
	Se3	(1×)	255.1(2)	Ta7–	Ta8	(2×)	291.8(1)
	Se4	(2×)	262.9(2)		Ta6	(2×)	304.6(1)
					Ta2	(1×)	348.1(1)
Ta3–	Ta6	(2×)	299.5(1)		Se5	(2×)	257.8(2)
	Ta2	(1×)	311.1(1)		Se7	(1×)	259.7(2)
	Ta4	(2×)	315.5(1)		Se4	(2×)	260.3(2)
	Ta1	(1×)	322.4(1)				
	Ta8	(1×)	339.2(1)	Ta8–	Ta7	(2×)	291.8(1)
	Ni	(2×)	250.3(2)		Ta3	(1×)	339.2(1)
	Se6	(1×)	258.7(2)		Se7	(2×)	258.5(2)
	Se8	(2×)	264.2(2)		Se8	(2×)	267.7(2)
					Se5	(1×)	267.7(2)
Ta4–	Ta4	(2×)	299.8(1)		Se6	(1×)	274.0(2)
	Ta1	(2×)	304.4(1)	Ni–	Ta1	(2×)	249.7(2)
	Ta3	(2×)	315.5(1)		Ta3	(2×)	250.3(2)
	Ta1	(1×)	350.4(1)		Ta2	(2×)	252.3(2)
	Ni	(1×)	284.2(3)		Ta4	(1×)	284.2(3)
	Se1	(2×)	261.3(2)		Ta6	(1×)	289.1(3)
	Se8	(1×)	264.2(2)		Ta5	(1×)	291.3(3)
	Se1	(1×)	270.9(2)		Se8	(1×)	363.8(3)
Se1–	Ta4	(2×)	261.3(2)	Se5–	Ta7	(2×)	257.8(2)
	Ta1	(2×)	265.4(2)		Ta8	(1×)	267.7(2)
	Ta4	(1×)	270.9(2)		Ta6	(1×)	278.2(2)
Se2–	Ta1	(1×)	257.4(2)	Se6–	Ta3	(1×)	258.7(2)
	Ta5	(2×)	258.8(2)		Ta6	(2×)	261.1(2)
					Ta8	(1×)	274.0(2)
Se3–	Ta2	(1×)	255.1(2)				
	Ta5	(2×)	257.8(2)	Se7–	Ta8	(2×)	258.5(2)
	Se4	(1×)	310.3(3)		Ta7	(1×)	259.7(2)
					Ta5	(1×)	301.6(2)
Se4–	Ta7	(2×)	260.3(2)				
	Ta2	(2×)	262.9(2)	Se8–	Ta4	(1×)	264.2(2)
	Ta6	(1×)	272.5(2)		Ta3	(2×)	264.2(2)
	Se3	(1×)	310.3(3)		Ta8	(2×)	267.7(2)

[a]Distances corresponding to $b = 344.2$ pm are not contained in the listings.

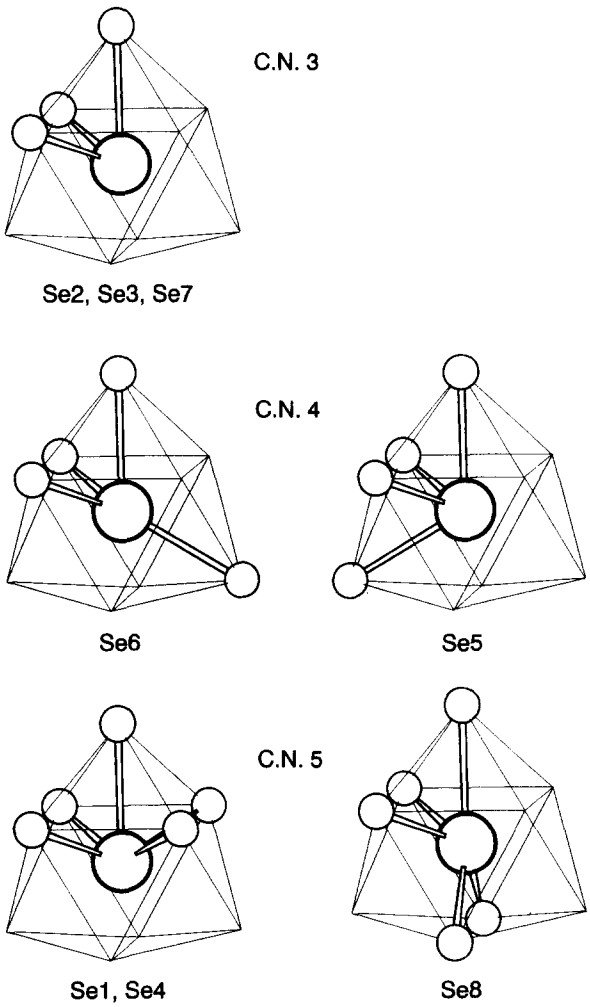

Fig. 7. Tantalum coordinations about selenium atoms depicted as fragments of an $SeTa_9$ tetrakaidecahedron.

in close van der Waals contact, we do not assume that the shrinkage is caused by any significant covalent bonding between Se3 and Se4. Similar short distances between sulphur atoms have been found in Ta_3S_2. Band structure calculations led to negative overlap populations for these close contacts (293 pm). The value of −0.039 was taken as an indicator of significant S–S repulsion [14].

6. Conclusions

The ternary selenides $CoTa_8Se_8$ and $NiTa_8Se_8$ are accessible from the elemental constituents by the application of high temperature synthesis techniques. The structure of $NiTa_8Se_8$ contains columnar intermetallic cores consisting of strongly metal–metal bonded, Ni-centred Ta_9 tetrakaidecahedra which are condensed into columns by shared triangulated prism faces. The selenium atoms cover the internal surface of the highly porous intermetallic framework, resulting in a one-sided coordination about the selenium atoms. The coordination polyhedra correspond to distinct fragments of a fictitious Ta_9Se tetrakaidecahedron. The concept of cluster condensation has been used to point out the relationship between the structures adopted by $Ni_{2-x}Nb_8S_{4+x}$, $Ni_2Ta_9S_6$, $Ni_2Ta_{11}Se_8$ and $NiTa_8Se_8$ and

the compositions of these phases. From this point of view the structure of $NiTa_8Se_8$ can be seen as an intermediate phase between $Ni_2Ta_{11}Se_8$ and "$NiTa_6Se_6$" which is not known as yet. This composition is expected for a quasi-one-dimensional material consisting of intermetallic columns of face-shared tetrakaidecahedra which are sheathed by chalcogen atoms. Such a compound remains an attractive target of further preparative studies.

Acknowledgments

This work was supported by the Deutsche Forschungsgemeinschaft, by the Ministerium für Wissenschaft and Forschung, NW and by the Fonds der Chemischen Industrie. We thank A. Roloff for measurements of single-crystal X-ray diffraction intensities.

References

1 M. Conrad and B. Harbrecht, *J. Alloys Comp., 187* (1992) 181.
2 J. L. Huang and B. G. Huang, *Acta Crystallogr. A, 46 (Suppl.)* (1990) C-287; W. Tremel, *Angew. Chem., Int. Edn. Engl., 103* (1991) 900; J. Neuhausen, K.-L. Stork, E. Potthoff and W. Tremel, *Z. Naturf. B, 47* (1992) 1203.
3 B. Harbrecht, *Angew. Chem., 101* (1989) 1696; *Int. Edn. Engl., 28* (1989) 1660.
4 X. Yao and H. F. Franzen, *J. Am. Chem. Soc., 113* (1991) 1426.
5 M. E. Badding and F. J. DiSalvo, *Inorg. Chem., 29* (1990) 3952; J. Li, R. Hoffmann, M. E. Badding and F. J. DiSalvo, *Inorg. Chem., 29* (1990) 3943.
6 M. Conrad and B. Harbrecht, *IVth Euro. Conf. on Solid State Chem., Dresden, Germany, September, 1992,* Gesellschaft Deutscher Chemiker, Book of Abstracts, p. 324.
7 B. Harbrecht, *J. Less-Common Met., 113* (1985) 349; B. Harbrecht, *J. Less-Common Met., 124* (1986) 125; M. J. Calhorda and R. Hoffmann, *Inorg. Chem., 27* (1988) 4679.
8 B. Harbrecht, *J. Less-Common Met., 141* (1988) 59.
9 B. Harbrecht, *Habilitationsschrift,* University of Dortmund, 1989; M. Conrad, *Diplomarbeit,* University of Dortmund, 1990.
10 R. D. Deslattes and A. Henins, *Phys. Rev. Lett., 31* (1973) 972.
11 K. Yvon, W. Jeitschko and E. Parthé, *J. Appl. Crystallogr., 10* (1977) 73.
12 K. L. Horovitz and V. A. Johnson, *Methods of Experimental Physics,* Vol. 6, Part B, *Solid State Physics,* Academic, New York, 1959, p. 33.
13 F. Kadijk, R. Huisman and F. Jellinek, *Acta Crystallogr. B, 24* (1968) 1102.
14 S.-J. Kim, K. S. Nanjundaswamy and T. Hughbanks, *Inorg. Chem., 30* (1991) 159.